Source-detector trajectory optimization for CBCT metal artifact reduction based on PICCS reconstruction

Sepideh Hatamikia [a,b,c,*], **Ander Biguri** [d], **Gernot Kronreif** [a], **Tom Russ** [e], **Joachim Kettenbach** [f], **Wolfgang Birkfellner** [c]

[a] Austrian Center for Medical Innovation and Technology (ACMIT), Wiener Neustadt, Austria
[b] Research center for Medical Image Analysis and Artificial Intelligence (MIAAI), Department of Medicine, Danube Private University, Krems, Austria
[c] Center for Medical Physics and Biomedical Engineering, Medical University of Vienna, Vienna, Austria
[d] Department of Applied Mathematics and Theoretical Physics, University of Cambridge, Cambridge, United Kingdom
[e] Computer Assisted Clinical Medicine, Heidelberg University, Heidelberg, Germany
[f] Institute of Diagnostic, Interventional Radiology and Nuclear Medicine, Landesklinikum Wiener Neustadt, Wiener Neustadt, Austria

Received 25 August 2022; accepted 6 February 2023

Abstract

Precise instrument placement plays a critical role in all interventional procedures, especially percutaneous procedures such as needle biopsies, to achieve successful tumor targeting and increased diagnostic accuracy. C-arm cone beam computed tomography (CBCT) has the potential to precisely visualize the anatomy in direct vicinity of the needle and evaluate the adequacy of needle placement during the intervention, allowing for instantaneous adjustment in case of misplacement. However, even with the most advanced C-arm CBCT devices, it can be difficult to identify the exact needle position on CBCT images due to the strong metal artifacts around the needle. In this study, we proposed a framework for customized trajectory design in CBCT imaging based on Prior Image Constrained Compressed Sensing (PICCS) reconstruction with the goal of reducing metal artifacts in needle-based procedures. We proposed to optimize out-of-plane rotations in three-dimensional (3D) space and minimize projection views while reducing metal artifacts at specific volume of interests (VOIs). An anthropomorphic thorax phantom with a needle inserted inside and two tumor models as the imaging targets were used to validate the proposed approach. The performance of the proposed approach was also evaluated for CBCT imaging under kinematic constraints by simulating some collision areas on the geometry of the C-arm. We compared the result of optimized 3D trajectories using the PICCS algorithm and 20 projections with the result of a circular trajectory with sparse view using PICCS and Feldkamp, Davis, and Kress (FDK), both using 20 projections, and the circular FDK method with 313 projections. For imaging targets 1 and 2, the highest values of structural similarity index measure (SSIM) and universal quality index (UQI) between the reconstructed image from the optimized trajectories and the initial CBCT image at the VOI was calculated 0.7521, 0.7308 and 0.7308, 0.7248 respectively. These results significantly outperformed the FDK method (with 20 and 313 projections) and the PICCS method (20 projections) both using the circular trajectory. Our results showed that the proposed optimized trajectories not only significantly reduce metal artifacts but also suggest a dose reduction for needle-based CBCT interventions, considering the small number of projections used. Furthermore, our results showed that the optimized trajectories are compatible with spatially constrained situations and enable CBCT imaging under kinematic constraints when the standard circular trajectory is not feasible.

Keywords: CBCT reconstruction; Needle-based interventions; Metal artifact reduction; Trajectory optimization

* Corresponding author.

Z Med Phys **xxx** (2023) xxx–xxx
https://doi.org/10.1016/j.zemedi.2023.02.001
www.elsevier.com/locate/zemedi

1 Introduction

Precise instrument placement is a critical step in all percutaneous needle-based interventional procedures, especially needle biopsies; this contributes to more accurate needle positioning and increases diagnostic accuracy [1,2]. With the increasing importance of minimally invasive treatments due to their efficacy and safety, the need for high-precision imaging has become paramount. C-arm cone beam computed tomography (CBCT) is a relatively new imaging technique that is frequently used in percutaneous procedures for lesions in soft tissue organs, e.g., liver and lung biopsies [3,4]. This modality allows real-time visualization of organs, low-dose scans, and is equipped with an open gantry that provides the user with flexibility for high-precision needle positioning even in technically challenging situations. For needle-based procedures, there is a need for an imaging modality that can accurately visualize the anatomy in close proximity to the needle to assess the appropriateness of needle placement during the procedure and allow for immediate adjustment in the case of misplacement. C-arm CBCT devices have the potential to provide such information intraoperatively. However, even with the most recent C-arm CBCT systems, capturing the exact needle position on the intraoperative CBCT image is challenging due to strong metal artifacts around the needle [5,6]. Refining the quality of intraoperative CBCT reconstructions for needle placement therefore holds great potential for improving target localization during interventions, allowing for immediate revision and thus reducing both the number of misdiagnoses and the need for subsequent biopsy interventions. Some strategies proposed in the literature to reduce metal artifacts in CBCT images are based on post-processing the acquired data in the projection domain [6,7]. In addition, optimal sinusoidal source-detector trajectories have recently been proposed to avoid artifacts originating from the metal parts of the imaged object, while still providing high coverage in the Radon space and its surroundings [8,9]. In recent years, it has been shown that nonconventional CBCT trajectories can have an impact on reducing metal artifacts and noncircular orbits can be used to avoid unfavorable projection views, thus significantly improving image quality near metal objects [8,10]. The authors in [11] proposed an on-the-fly orbit optimization approach to improve the image quality of the reconstruction in the presence of artifacts caused by metal screws during spine surgery. They performed the adjustments using a Convolutional Neural Network (CNN) during the scan and regressed an image quality metric over all possible next projections of the current X-ray image. Adjusting the scan trajectory to achieve optimal projection views resulted in non-circular source-detector trajectories that avoided poor images and improved imaging performance, especially with respect to metal artifacts. In [12], a method to reduce the effects of metal artifacts by prospectively defining the source-detector orbits of the C-arm was proposed. Their proposed method could mitigate metal-related distortions in the projection data and did not require accurate prior information about the patient or metal implants. Their approach involved coarse localization of metal objects, model-based approximation of metal-induced X-ray spectral shift related to possible trajectories, and detection of optimized orbits to reduce spectral shift variation.

In [8,13,14] non-circular trajectories were proposed to maximize data completeness in the presence of metal. The main goal was to use X-rays that pass through the target object but avoid X-rays that pass through the metal object for the reconstruction. They proposed a local metric for data completeness based on Tuy's condition. Their measure accounts for the presence of metal object by counting the percentage of great circles which are sampled by an individual trajectory. In another study using the same image quality metric [9], optimized non-circular orbits were designed in simulations with the goal of maximizing Tuy's condition in the presence of metal objects. The trajectories they designed showed a remarkable reduction in metal artifacts and also a significant visibility of in-plane structures that would be obscured by the metal object. Their approach was also resilience when having multiple metal objects. The common reconstruction methods in literature used for CBCT trajectory optimization are penalized-likelihood reconstruction [9,11,24] and total variation regularized methods, such as adaptive steepest descent projection onto convex set (ASD-POCS) [19,20]. In [15], the authors reported a significant reduction in artifacts and improvement in CT image quality in hip replacement patients using a Prior Image Constrained Compressed Sensing (PICCS)-based algorithm. In addition, in [16], the authors developed a PICCS CT-based iterative reconstruction algorithm based on a superiorization method to reduce metal artifacts. Their algorithm used a previous image reconstructed with the normalized metal artifact reduction technique and could remove the most severe streaking artifacts originating by metal objects. Furthermore, in [17,18], the authors reported the high performance of the PICCS method for cardiac interventional imaging when using an under-sampled projection acquisition using CBCT device. In the studies [15–18], the proposed PICCS reconstruction-based methods were either developed and validated for CT imaging [15,16], or no metal object was included [17,18]. In addition, PICCS algorithm was never used in CBCT imaging together with trajectory optimization.

In this study, we validated the performance of the sparse-view PICCS reconstruction combined with customized three-dimensional (3D) source-detector CBCT trajectories to reduce metal artifacts in needle-based

Please cite this article as: S. Hatamikia, A. Biguri, G. Kronreif et al., Source-detector trajectory optimization for CBCT metal artifact reduction based on PICCS reconstruction, Z Med Phys, https://doi.org/10.1016/j.zemedi.2023.02.001

procedures where a prior standard CBCT is available. An anthropomorphic thorax phantom into which a needle was inserted was used to verify the proposed approach. To our knowledge, this is the first study to investigate the possibility of reducing metal artifacts with the PICCS algorithm in needle-based CBCT procedures. In addition, the combination of sparse-view PICCS reconstruction with optimal 3D projection views has not yet been investigated. We also evaluated the performance of the PICCS algorithm in reconstructing unconventional trajectories under kinematic constraints where a standard circular trajectory is not possible.

2 Materials and methods

This section explains the pipeline used for the proposed metal artifact reduction and trajectory optimization using the PICCS algorithm. In section 2.1, the general workflow of the proposed method is presented in a high-level overview. Section 2.2 introduces the C-arm CBCT device used in this work, and the data acquisition. Section 2.3 describes how the projection data has been simulated with approximation of real noise sources. Section 2.4 briefly introduces the PICCS image reconstruction algorithm and section 2.5 introduces three different trajectory optimization procedures that are evaluated in this work. A brief comment in computational implementation of PICCS is introduced in 2.6. Finally, section 2.7 introduces all the experimental setting for the scanner experiment results.

2.1 Workflow for metal artifact reduction based on PICCS algorithm and customized CBCT trajectories

In our proposed workflow (Fig. 1), we suggest creating a case-specific model from a prior standard CBCT. This CBCT scan is acquired at the beginning of the procedure before needle placement and serves as a prior image used for PICCS reconstruction of the subsequent CBCT scans. First, a simulation where a needle is digitally inserted into the prior CBCT is performed, using information about the position of the needle provided by the surgeons, derived from surgery planning stage. This prior CBCT with the digitally inserted needle is used as a digital phantom for trajectory simulation and target delineation. A set of possible X-ray source-detector trajectories is then defined, taking into account the kinematic constraints of the imaging device and the treatment room. In an optimization procedure (Section 2.5), synthetic digitally rendered radiographs (DRRs) of projections for the defined source-detector trajectories are generated, reconstructed using the PICCS algorithm, and quantitatively evaluated to find the best trajectory with the highest value of an objective function. After placing the needle in the real situation (similar position as the digitally inserted needle), the optimized trajectory selected in the simulation phase is applied to the CBCT device to acquire real projections for reconstruction.

2.2 Imaging device and data acquisition

In this study, we used a Philips Allura FD20 Xper C-arm with 1195 mm source-detector distance, 810 mm source-axis distance, and a 30×40 cm^2 detector with 0.776 mm pixel pitch. This device can rotate by angle $\theta 1$ toward right anterior oblique (RAO)/left anterior oblique (LAO) direction while having an oblique ψ at different cranial (CRA)/caudal (CAU) angles. It is also able to rotate by angle $\theta 2$ toward CRA/CAU direction while having an oblique φ at different RAO/LAO angles [19].

For data acquisition, the space of possible positions is derived from spatial constrains of the setup. Considering the needle inserted into the phantom, RAO/LAO rotation with a maximum oblique ψ of 20° was feasible in both CRA and CAD directions. Additional constraints due to other medical devices and patient table might also occur in a clinical setting. To mimic such constraints, an arbitrary "forbidden area" is introduced into the spatial range of possible trajectories, similar to our previous study [19,20]. These kinematic constraints will be taken into account when designing the optimized trajectories (Section 2.5) so that the trajectory does not include the forbidden region. The defined forbidden area used in this study was chosen based on a realistic case scenario in clinic and serves to demonstrate the flexibility of the chosen trajectory in handling and selecting the angular range outside a defined collision area. This approach has been used in our two previous studies [19,20] to develop collision avoidance customized trajectories. Based on our approach, the trajectory search space is defined as all possible regions where the device can rotate in 3D space, except the defined forbidden region, and then trajectories that do not interface with such a collision region (according to where this forbidden region is defined or its shape or size) are defined (e.g., sinusoidal trajectories or combinations of multiple arcs (Section 2.5)). Then, the optimized trajectories can be determined from those possible trajectory options. The generalization of collision areas has already been investigated and proved in our previous study [20] where two different forbidden areas with different size and shape were simulated.

2.3 Projection simulation

In order to create synthetic projections, Poisson noise was added and Bare-beam fluence was modeled with $I_0=10^4$ photons per detector element as in our previous study [19], approximating device exposure with 350 mAs and beam energy of 80 kV. Source-detector and source-isocenter distances were set to 1195 mm and 810 mm respectively,

Please cite this article as: S. Hatamikia, A. Biguri, G. Kronreif et al., Source-detector trajectory optimization for CBCT metal artifact reduction based on PICCS reconstruction, Z Med Phys, https://doi.org/10.1016/j.zemedi.2023.02.001

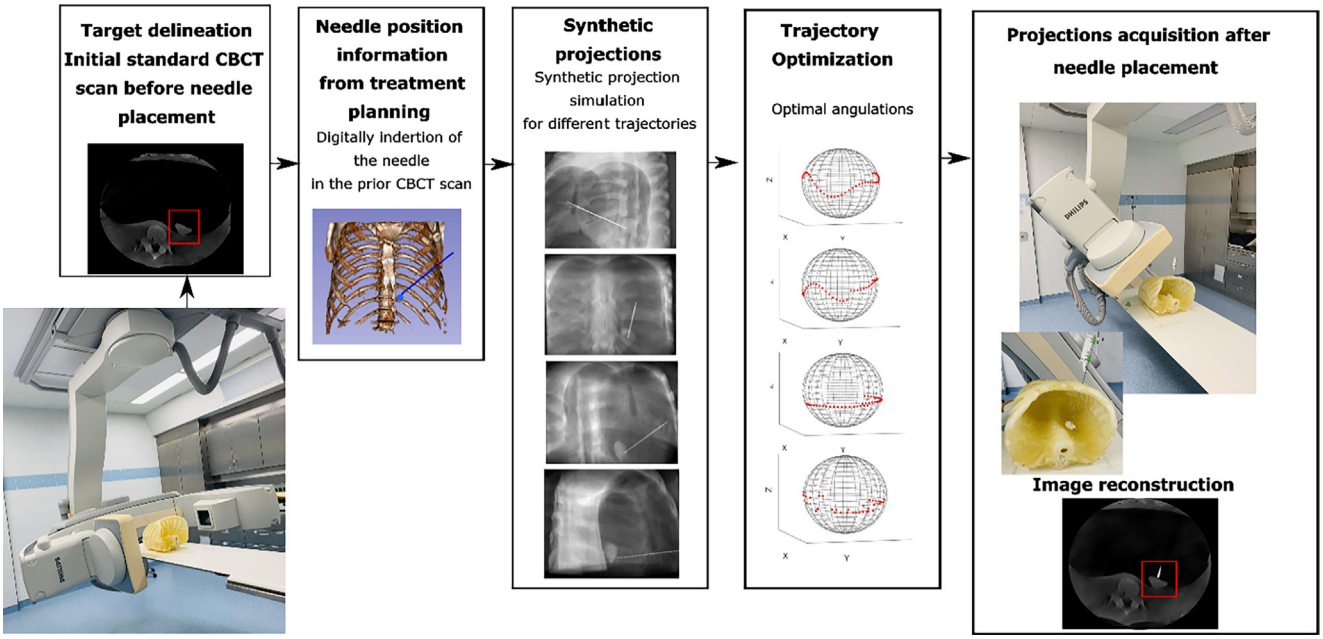

Figure 1. Schematic of the workflow for our proposed customized CBCT imaging with the goal of needle-based metal artifact reduction. A prior standard CBCT is acquired and used as a digital phantom for simulation. A needle is digitally inserted into the digital phantom and different possible trajectories are simulated. The trajectory with the optimal angulation is selected and implemented on the C-arm. Real projection data is then used to reconstruct the final image.

corresponding to the geometry of the Philips Allura FD20 Xper C-arm device. All DRRs included a 30 × 40 cm^2 detector size and 0.776 mm pixel pitch was simulated to match with the detector specifications. The forward projections were simulated using the ray-driven method based on graphics processing unit (GPU) implementation using the hardware-accelerated trilinear interpolation [26]. The needle was digitally introduced into the image from the phantom obtained by CBCT previously (including tumor models (see Section 2.7.1)) using the CurveMaker module in 3D Slicer. Photon starvation and beam hardening [27,28] were also simulated to replicate the effect of metal artifacts on the reconstructed image.

To simulate the photon starvation, the digitally inserted metal needle was segmented from the original CBCT image and an image containing only the needle was created. Forward projection was applied to both the original CBCT image with the digital needle and the image including only the segmented needle, and the created projections were compared. Finally, the pixel values related to projected needle in the image containing only needle were determined and set to zero in the projections created from the original CBCT. We also used a simplified approach to simulate the beam hardening effect. Three volumes were simulated, each one corresponding to a different photon energy. To approximate the real projections as closely as possible, the spectral attenuation coefficients of the needle voxels were determined empirically, comparing the images with the real measured and reconstructed images. Then, the projections from the volumes were averaged to obtain the simulated data with beam hardening.

2.4 PICCS image reconstruction

The PICCS algorithm comes from a Compressed Sensing (CS) formulation of the reconstruction problem. Given a linear system of equations

$$Ax = b + \tilde{e}, \tag{1}$$

where x is a lexicographically ordered vector of an image, b is the lexicographically ordered vector of the measured projections,A is a linear system model that describes the x-ray transform and $\tilde{e}$ is the error, a CS objective function can be proposed as

$$\underset{x}{\operatorname{argmin}} |\psi x|_1, \quad \text{s.t. } Ax = b, \tag{2}$$

where ψ is some sparsifying transform. Typically, in medical CT this transform is the discrete gradient operator, as humans tend to have small L^1-norm of the image gradient, thus tend to have very sparse image gradients. The L^1 norm of the discrete gradient is commonly referred to as the total variation (TV). For example, the well-known ASD-POCS is formulated in this way [21].

Please cite this article as: S. Hatamikia, A. Biguri, G. Kronreif et al., Source-detector trajectory optimization for CBCT metal artifact reduction based on PICCS reconstruction, Z Med Phys, https://doi.org/10.1016/j.zemedi.2023.02.001

PICCS builds on this formulation by introducing a prior image, x_p and instead uses the following function

$$\underset{x}{\operatorname{argmin}} |(1-\alpha)(\psi(x-x_p))|_1 + |\alpha(\psi x)|_1, \quad \text{s.t. } Ax = b, \tag{3}$$

where α is a parameter that controls the strength of the prior image constraint. In this work, we solve the above equation using the ASD-POCS algorithm too. At $\alpha = 1$, the method becomes a purely TV minimizing algorithm, as in the original ASD-POCS work. In this work, α= 0.08.

2.5 Trajectory optimization methods

Several trajectory optimization approaches have been proposed in the literature [10] for customizing CBCT trajectories, including simple optimization methods such as greedy [22,14] and brute force [11,19] to heuristic methods such as covariance matrix adaptation evolution strategy (CMA-ES) [23] and genetic algorithm (GA) [24] or combination of brute force and heuristic approaches [20].

In this study, we investigated the performance of four different trajectory optimization methods; the first two methods are proposed in this work and the other two methods have already been proposed in the literature. As the objective function, we used the value of structural similarity index measure (SSIM) [25] to evaluate the performance of the trajectories in the simulation phase for all optimization methods. The number of projections for each optimized trajectory was set to 20 in this study.

2.5.1 Method 1

In this method, we search for the best combination of the short sinusoid trajectories which gives the highest reconstruction performance in a pre-defined VOI. A series of 150 sinusoids with the entire possible rotation range at different random frequencies are simulated taking into account the possible range of the device movement. The sinusoid trajectories are divided into defined number of parts (in this study two parts) to provide higher flexibility in the presence of unavoidable kinematic constraints. Then, DRRs related to those short trajectories are simulated on the CBCT-based digital phantom and image reconstruction step is then performed for the entire set of short sinusoid trajectories and the objective function is calculated in the VOI, selecting the short trajectory with best value. The selected first short trajectory is eliminated from the search list, appended to all other short trajectories in the search space, and the algorithm is run again to find the second-best short sinusoid trajectory. The combination of the best two short sinusoid trajectories is returned as the optimized trajectory. The optimization steps are summarized in Method 1. This approach is similar to Method 3 (Section 2.5.3) [19] with the difference that best combination of the short sinusoid trajectories are used instead of combination of normal short arcs.

Method 1: Trajectory optimization
Input: Search space; possible projections
Step 1: Define a set of sinusoid trajectories at different random frequencies which are feasible considering the real device movement range and other
Step 2: Divide each sinusoid trajectory into two parts
Step 2: Simulate projections for all defined short sinusoid trajectories on the prior CBCT digital phantom
Step 3: FOR 1: number of short trajectories

- Reconstruct the image using the set of DRRs related to the corresponding short trajectory
- Crop the reconstructed image at the VOI
- Calculate the objective function at the cropped area

ENDFOR
Step 4: Find the best short sinusoid candidate which can maximize the objective function and remove it from the search space
Step 5: Append best candidate to all other short sinusoid trajectories in the
search space
Step 6: find the second-best short trajectory which its combination with the first trajectory maximizes the objective function by repeating Step 3 and Step 4
Step 7: Return selected trajectory (combination of two short sinusoid trajectories)

2.5.2 Method 2

This method uses orbits that are a continuous function of the rotation angle θ1 and gantry tilt ψ. A simple parameterization as proposed in [24] is used which involves periodic basis functions using constant, sine, and cosine terms:

$$\psi(\theta 1) = \sum_{i=1}^{k} \Omega_i b_i(\theta 1), \quad b_1(\theta 1) = 1, \; b_2(\theta 1) = \sin\theta 1,$$
$$b_3(\theta 1) = \cos\theta 1, \; b_4(\theta 1) = \sin 2\theta 1, \cdots, \tag{4}$$

Initial Ω set with k random values:

$$\Omega = rand[-1, +1] \tag{5}$$

Where *rand* is the random operator that selects random values between the given range (in this study between -1 and +1).

Replacement set of Ω values to investigate further optimization of the trajectory:

$$\Omega_{update} = \{-1 : 0.1 : +1\} = \{-1, -0.9, -0.8 \cdots, +1]\} \tag{6}$$

We propose to create a set of 150 trajectories, each with k Ω values (k=9 in this work), randomly selected from the range with values between -1 and +1 (Eq. (5)) taking into

Please cite this article as: S. Hatamikia, A. Biguri, G. Kronreif et al., Source-detector trajectory optimization for CBCT metal artifact reduction based on PICCS reconstruction, Z Med Phys, https://doi.org/10.1016/j.zemedi.2023.02.001

account the possible range of the device movement and available kinematic constraints. The DRRs associated with these trajectories are simulated on the CBCT-based digital phantom. Image reconstruction is then performed for the entire set of trajectories, the objective function in VOI is calculated, and the trajectory with the best value is selected. In a second optimization step, we then search for a possible improvement of the selected trajectory by sequentially optimizing the Ω values. We start with the first Ω value from the initial Ω set (Eq. (5)) of the selected trajectory and replace this value with all values from the set of updated Ω values (Ω_{update}, Eq. (6)). If by replacing any of values from the updated Ω set (Eq. (6)) an increase in the objective function is detected, that new Ω value from Eq. (6) is replaced by the first initial value in Eq. (5). This procedure is repeated for other Ω values from the initial set until an increase in the objective function is found. Once there is no more improvement in the objective function, the k updated Ω values are returned for the final optimal trajectory. The optimization steps are summarized in Method 2.

Method 2: Trajectory optimization
Input: Search space, possible projections
Step 1: Define a set of possible arbitrary trajectories with k random Ω values (values are set randomly a number between -1 to +1, Eq. (5))
Step 2: Simulate projections for all defined trajectories on the prior CBCT digital phantom
Step 3: FOR 1: number of trajectories

- Reconstruct the image using the set of DRRs related to the corresponding trajectory
- Crop the reconstructed image at the VOI
- Calculate the objective function at the cropped area

ENDFOR
Step 4: Find the trajectory with maximum score
Step 5: WHILE new Ω value increases the objective function score
Step 6: FOR 1: number of initial Ω (k)

- Check whether replacement of any new Ω value from the range (-1: 0.1 :+1) (Eq. (6)) with the initial omega value (Eq. (5)) increases the objective function, if yes replace that with the initial Ω value

END
END
Step 7: Return selected trajectory (optimized trajectory)

2.5.3 Method 3

We used the same optimization method as in [19], in which the authors proposed to use a VOI from an existing diagnostic CT scan and simulated a wide variety of possible trajectory combinations from short arcs on this prior CT, taking into account kinematic constraints in the operating room. In this method two types of rotations (rotation toward RAO/LAO direction while having a tilt at various fixed CRA/CAU angles and rotation toward CRA/CAU direction while having a tilt at various fixed RAO/LAO angles) were implemented. Each of the resulting rotation is divided into a certain number of short arcs (in this study two short arcs) and the final trajectory consists of combination of two of such arcs. Through an optimization process, possible arcs are selected, reconstructed with iterative algorithms, and quantitatively evaluated to find the combination of short arcs that best fits the selected objective function. This process is repeated for optimization. In detail, first, a VOI is selected where the image quality is to be optimized. Then, synthetic projections are simulated using the CT-based digital phantom for all defined short arcs. An image reconstruction step is then run for the entire set of possible short arcs and an objective function (image quality metric) is evaluated in the VOI selecting the arc with best value. The selected short arc is removed from the search list, appended to all other available arcs in the search space, and the algorithm is rerun as many times as required. The main goal of trajectory optimization in this study was to enable CBCT imaging in scenarios with kinematic constraints (e.g., originating from other medical devices or patient table) where a standard circular trajectory is not feasible. In this work, a similar approach to Method 1 (Section 2.5.1) has been proposed, with the difference that short sinusoids are combined instead of short arcs to create the final optimized trajectory.

2.5.4 Method 4

We also used the same optimization approach as in [22]. In [22] the authors proposed a function whose maximum identifies the next best projection view based on task detectability. The detectability index of the non-prewithening matched filter observer (NPWMF) observer for a specific task, which can be written in the Fourier-domain, was used to assess the candidate trajectory. For the optimization process, the authors tried to find the best projection views using a sequential optimization method. They found high performing sets of projection views using a greedy method where new angles were added to a growing set of projection angles that started with an empty set. Therefore, a set of projection angles is composed by iteratively finding the next most valuable projection in the detectability map and adding it to the existing set of projection angle pairs. In this study, we used the same greedy optimization process as introduced in [22], however, SSIM value was used to evaluate the performance of the trajectories in the simulation phase.

Please cite this article as: S. Hatamikia, A. Biguri, G. Kronreif et al., Source-detector trajectory optimization for CBCT metal artifact reduction based on PICCS reconstruction, Z Med Phys, https://doi.org/10.1016/j.zemedi.2023.02.001

2.6 Computational time

We modified the implementation of PICCS in the Tomographic Iterative GPU-based Reconstruction (TIGRE) toolbox [29] to run the reconstruction fully on the GPU. This implementation takes approximately 1.50 second and 2.35 seconds for each PICCS reconstruction (with five iterations), including 20 and 40 projections, respectively, using a computer with an NVIDIA GeForce RTX 2080 and a 32-core Advanced Micro Devices (AMD) processor.

2.7 Experimental methods

This section describes the experimental tools used for the validation of our method. First, chest phantoms are described (Section 2.7.1), then the image quality metrics to evaluate the results (Section 2.7.2) and finally a description of the experimental setup is given (Section 2.7.3).

2.7.1 Phantoms

Two 3D printed (PolyJet) objects serving as tumor (target 1 and 2) were placed inside two different regions of the thorax phantoms and were considered as the imaging targets to be optimally reconstructed. We evaluated the performance of reconstruction at these two imaging targets using an in-house built anthropomorphic thorax phantom developed previously by our group [30]. The thorax phantom including the biopsy needle and one tumor, and a CT from the phantom with the two imaging target regions is shown in Fig. 2.

2.7.2 Image quality metrics

SSIM and universal quality index (UQI) were used as the image quality metrics in order to evaluate the performance of the reconstructed images using different trajectories based on real projection data. The values of these two metrics were computed between the VOI from the reconstruction image from the optimized trajectories and the reference image (ground truth) was defined as the prior CBCT image with the digitally inserted needle (Section 2.1).

2.7.3 Physical experiments

We realized the selected optimized trajectories achieved from the trajectory optimization phase (Section 2.5) with a step-and-shoot protocol on the imaging device by positioning the C-arm at each projection angle. The reconstruction results from the optimized trajectories based on real projections (including 20 projections) using the PICCS reconstruction were compared with the standard circular trajectory of the C-arm (313 projections over a rotation of 210°) using the Feldkamp, Davis, and Kress (FDK) reconstruction algorithm, which is widely used commercially. In addition, the results of the optimized trajectories using the PICCS method were compared to a sparse-view circular trajectory using the FDK method including same number of projections as for the optimized trajectories (20 projections). For further analysis, we also performed a comparison with CBCT images reconstructed with the PICCS algorithm but from a sparse-view circular trajectory including 20 projections. This comparison was performed to investigate whether an improvement in reconstruction results could be achieved when using optimized sparse-view 3D projections compared to the circular sparse-view circular projections when using the PICCS as the reconstruction method. In addition, a comparison of the results with ASD-POCS method using 20 projections was also performed. The ASD-POCS method was chosen for comparison because it has been shown to be very efficient in reconstructing images in cases with limited projection views [19,20,31].

3 Experimental results

In this section, the experimental results of the different trajectory optimization methods are explained. Section 3.1 presents the obtained optimized trajectories and the corresponding 3D visualization. Section 3.2 describes the reconstruction results and the corresponding quantitative results using two image quality metrics.

3.1 Trajectory optimization results

The 3D visualizations of the optimized trajectories of all 4 optimization methods (Section 2.5) for the two image targets are shown in Figs. 3 and 4. In all cases, the optimized trajectories did not include the forbidden area (yellow rectangle in Figs. 3 and 4). For target 2, the two selected short arcs have the same angular tilt, which is why they appear as one continuous long arc in Fig. 4.

3.2 Physical experiment results

The reconstruction results of the standard circular trajectory with FDK algorithm and 313 projections, the sparse-view circular trajectory with FDK algorithm and 20 projections, the sparse-view circular trajectory with ASD-POCS algorithm and 20 projections, the sparse-view circular trajectory with PICCS algorithm and 20 projections, the optimized trajectories based on PICCS algorithm, 20 projections and methods 1-4 for target 1 and target 2 are shown in Figs. 5 and 6. In addition, the ground truth images (prior CBCT with digitally inserted needle) are provided for both targets to facilitate visual assessment and comparison of performance of the reconstructed images. For target 1 and target 2, all images reconstructed with the PICCS algorithm showed significantly better visualization of the tumor and needle than images reconstructed with the circular trajectory using FDK methods (both using 313 and 20 projec-

Please cite this article as: S. Hatamikia, A. Biguri, G. Kronreif et al., Source-detector trajectory optimization for CBCT metal artifact reduction based on PICCS reconstruction, Z Med Phys, https://doi.org/10.1016/j.zemedi.2023.02.001

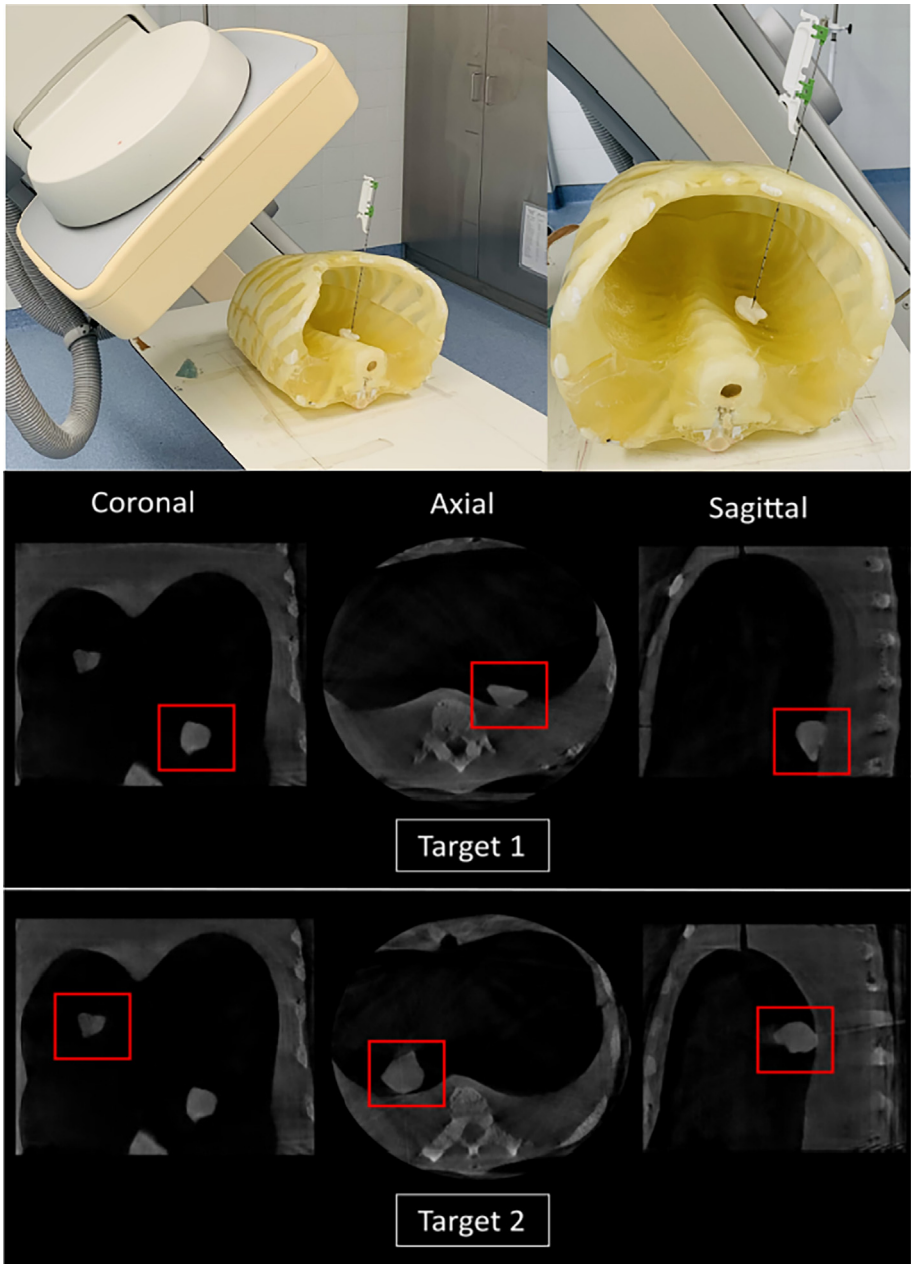

Figure 2. The in-house developed thorax phantom including a biopsy needle pushed through the chest into the target on the left side and one printed tumor model from two views (upper row), a CT from the phantom with the imaging target (middle row) and imaging target 2 (lower row).

tions) and with the ASD-POCS method (20 projections). The calculated SSIM and UQI values also confirmed the visual inspection results, as both image quality metrics showed higher values for images reconstructed with the PICCS algorithm (20 projections) compared to images reconstructed with ASD-POCS and the FDK algorithm, even when 313 projections were used using FDK method (Table 1).

For target 1, the highest values of SSIM and UQI for images from PICCS algorithm were achieved 0.7301, 0.7080 and 0.7521, 0.7308 and 0.7109, 0.7301 when using optimization methods 2, 3 and 4, respectively. In addition, for target 2, the highest values of the same image quality metrics using PICCS algorithm were obtained 0.7121, 0.6544 and 0.7308, 0.7248 and 0.7217, 0.6864 when using optimization methods 2, 3 and 4, respectively.

Please cite this article as: S. Hatamikia, A. Biguri, G. Kronreif et al., Source-detector trajectory optimization for CBCT metal artifact reduction based on PICCS reconstruction, Z Med Phys, https://doi.org/10.1016/j.zemedi.2023.02.001

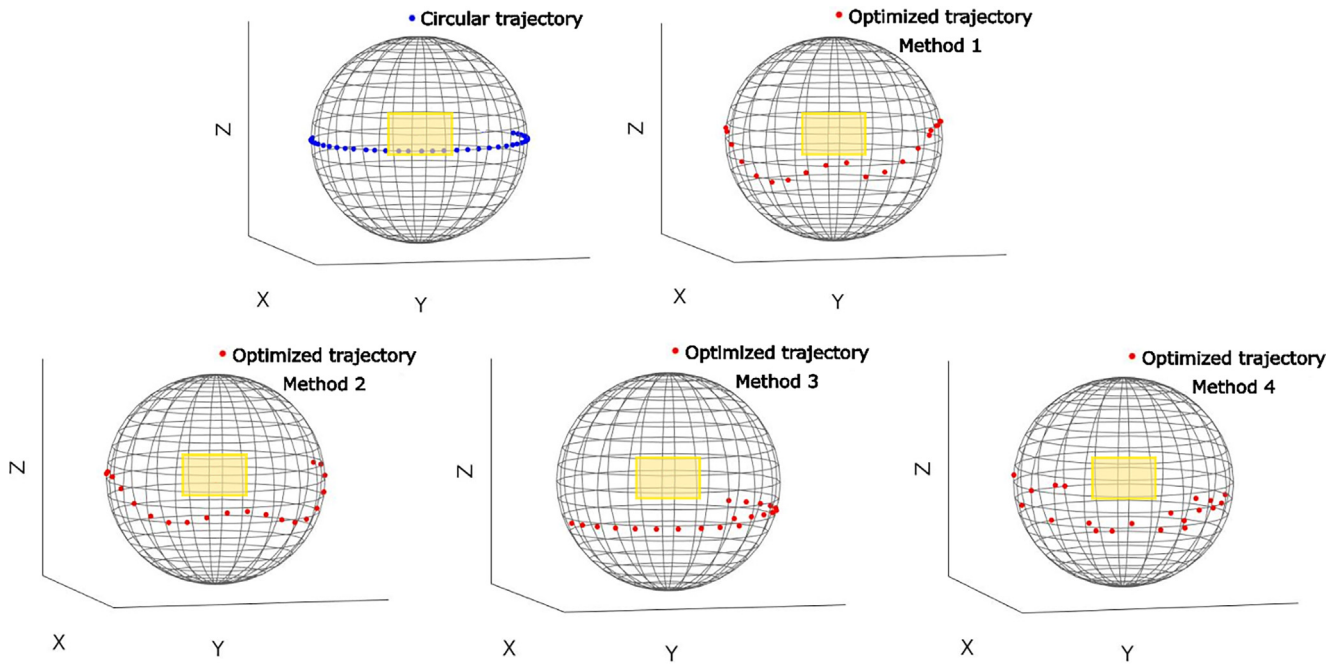

Figure 3. Three-dimensional visualization of the circular trajectory and optimized trajectories (Methods 1-4) for imaging target 1. The yellow rectangle represents the forbidden area.

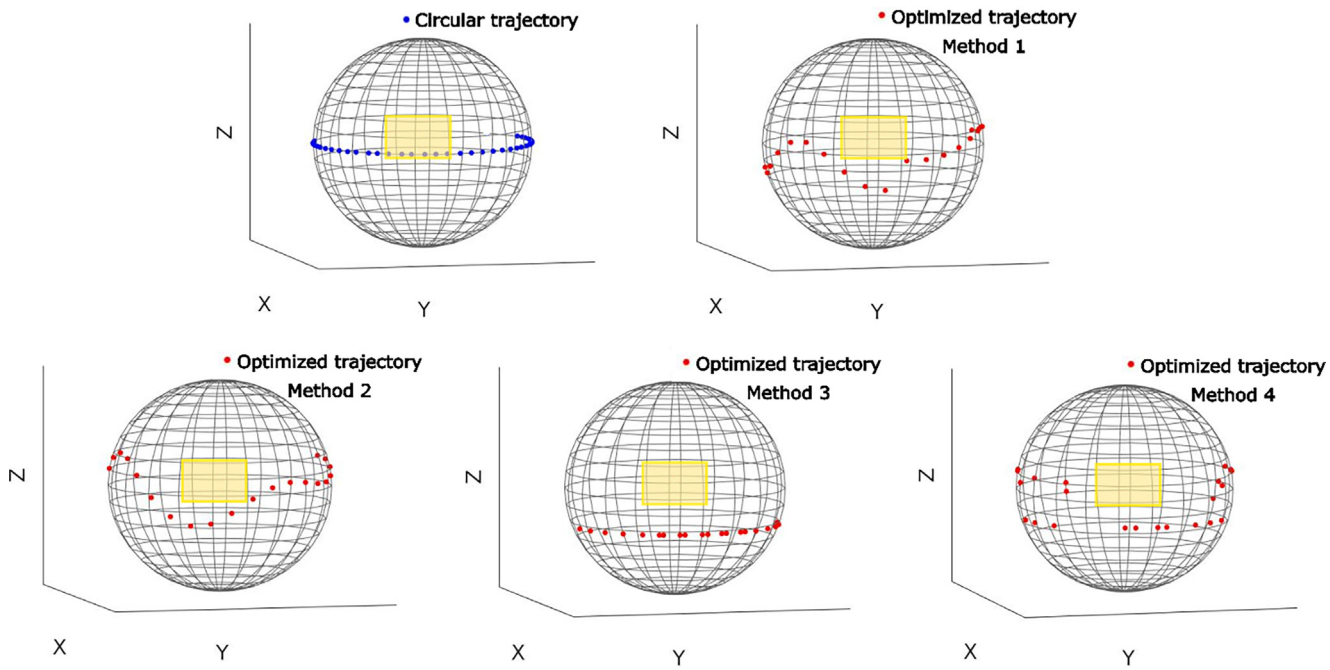

Figure 4. Three-dimensional visualization of the circular trajectory and optimized trajectories (Methods 1-4) for imaging target 2. The yellow rectangle represents the forbidden area.

For both imaging targets, reconstructed images based on PICCS algorithm and optimization Method 3 achieved the highest value for both image quality indexes among different optimization methods. When comparing the results from sparse-view circular trajectory and sparse-view optimized trajectory both using PICCS algorithm and the same

Please cite this article as: S. Hatamikia, A. Biguri, G. Kronreif et al., Source-detector trajectory optimization for CBCT metal artifact reduction based on PICCS reconstruction, Z Med Phys, https://doi.org/10.1016/j.zemedi.2023.02.001

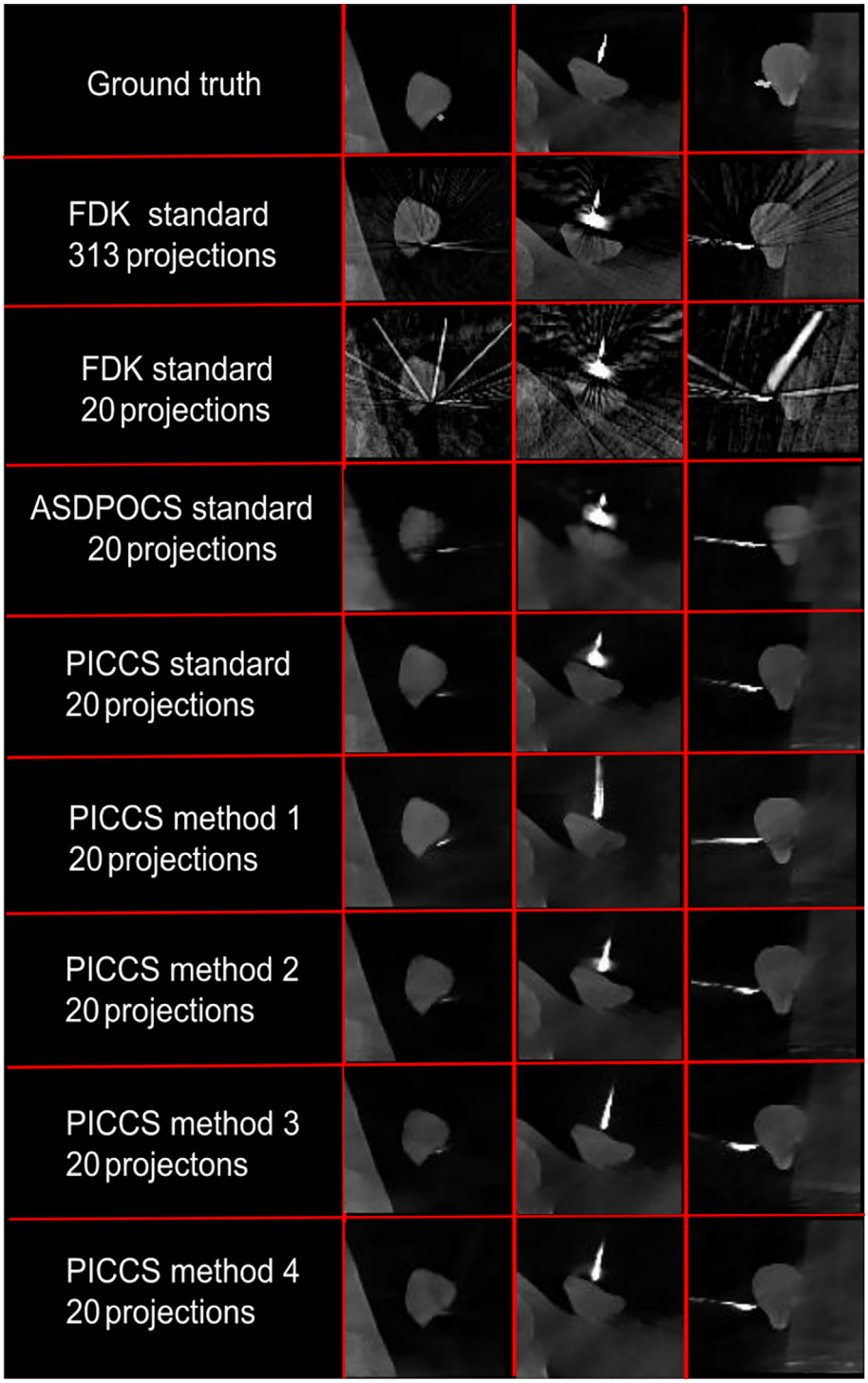

Figure 5. Reference image for target 1, reconstruction results for the imaging target 1 related to standard circular trajectory with FDK algorithm and 313 projections, the sparse-view circular trajectory with FDK algorithm and 20 projections, the sparse-view circular trajectory with ASD-POCS algorithm and 20 projections, the sparse-view circular trajectory with PICCS algorithm and 20 projections, the optimized trajectories based on PICCS algorithm, 20 projections and methods 1-4. The display window shows linear attenuation coefficient and is set to the gray value range [0–10].

Please cite this article as: S. Hatamikia, A. Biguri, G. Kronreif et al., Source-detector trajectory optimization for CBCT metal artifact reduction based on PICCS reconstruction, Z Med Phys, https://doi.org/10.1016/j.zemedi.2023.02.001

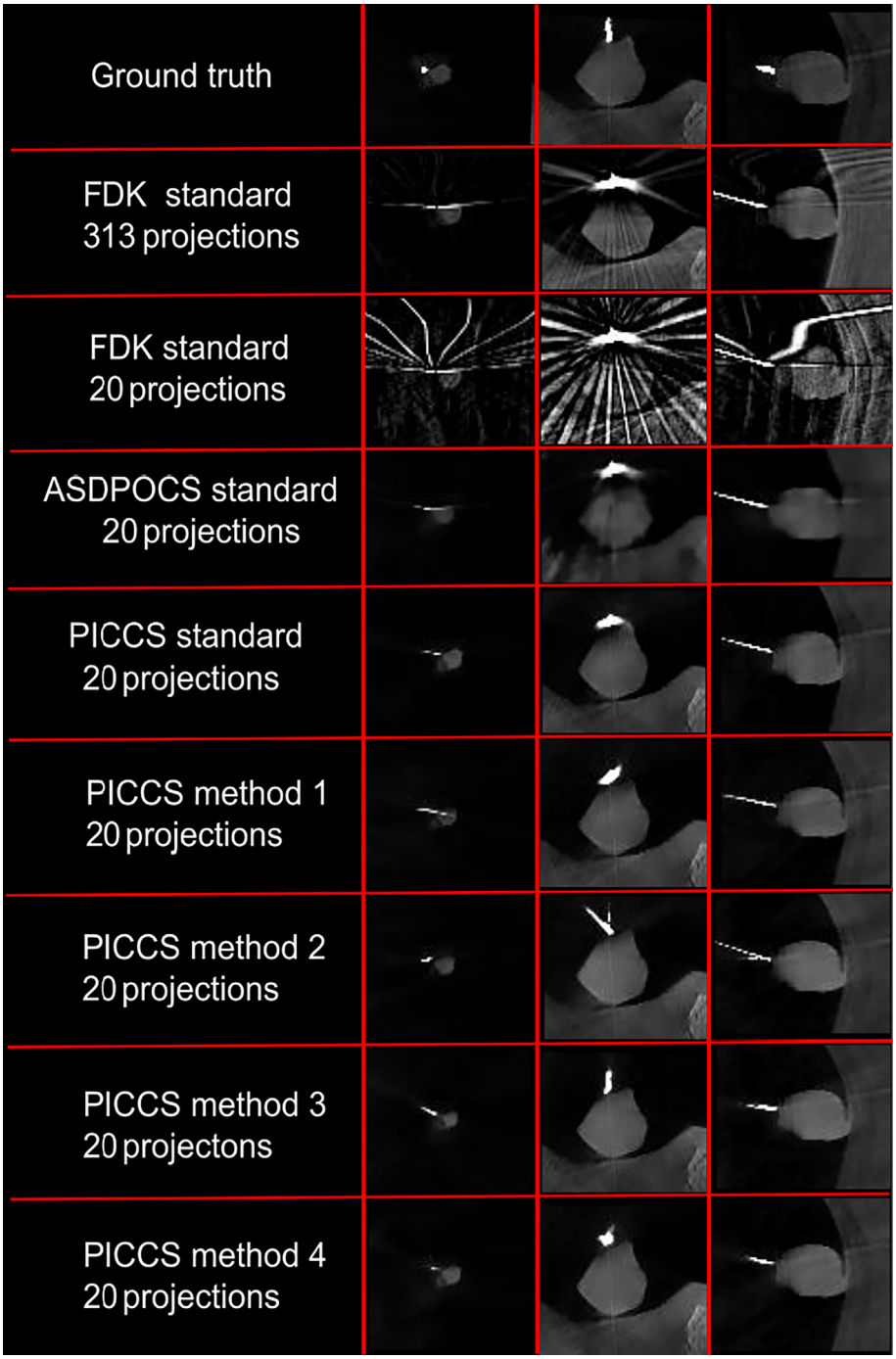

Figure 6. Reference image for target 2, reconstruction results for the imaging target 2 related to (a) standard circular trajectory with FDK algorithm and 313 projections, the sparse-view circular trajectory with FDK algorithm and 20 projections, the sparse-view circular trajectory with ASD-POCS algorithm and 20 projections, the sparse-view circular trajectory with PICCS algorithm and 20 projections, the optimized trajectories based on PICCS algorithm, 20 projections and methods 1-4. The display window shows linear attenuation coefficient and is set to the gray value range [0–10].

projection number (20 projections), we observed that for most of images using the trajectory optimization methods, a higher accuracy was achieved compared to the sparse-view circular trajectory using PICCS method. The total computational time for optimization methods 1, 2, 3, and 4 was 8.98, 7.79, 3.56 and 11.65 minutes respectively. In addition,

Please cite this article as: S. Hatamikia, A. Biguri, G. Kronreif et al., Source-detector trajectory optimization for CBCT metal artifact reduction based on PICCS reconstruction, Z Med Phys, https://doi.org/10.1016/j.zemedi.2023.02.001

Table 1
The values related to the structural similarity index measure (SSIM) and universal quality index (UQI) metrics between the reconstructed image from different trajectories and the reference CBCT for imaging target 1 and target 2.

Trajectory	Image quality metric type	Image quality metric value Target 1	Image quality metric value Target 2
FDK circular	SSIM	0.5610	0.5189
313 projections	UQI	0.6054	0.4603
FDK circular	SSIM	0.3580	0.2819
20 projections	UQI	0.3925	0.2323
ASD-POCS circular	SSIM	0.5510	0.6035
20 projections	UQI	0.6236	0.5448
PICCS circular	SSIM	0.7049	0.6860
20 projections	UQI	0.6752	0.6263
PICCS method 1	SSIM	0.6515	**0.7121**
20 projections	UQI	0.6927	**0.6544**
PICCS method 2	SSIM	**0.7301**	0.6538
20 projections	UQI	**0.7080**	0.6307
PICCS method 3	SSIM	**0.7521**	**0.7308**
20 projections	UQI	**0.7308**	**0.7248**
PICCS method 4	SSIM	**0.7109**	**0.7217**
20 projections	UQI	**0.7301**	**0.6864**

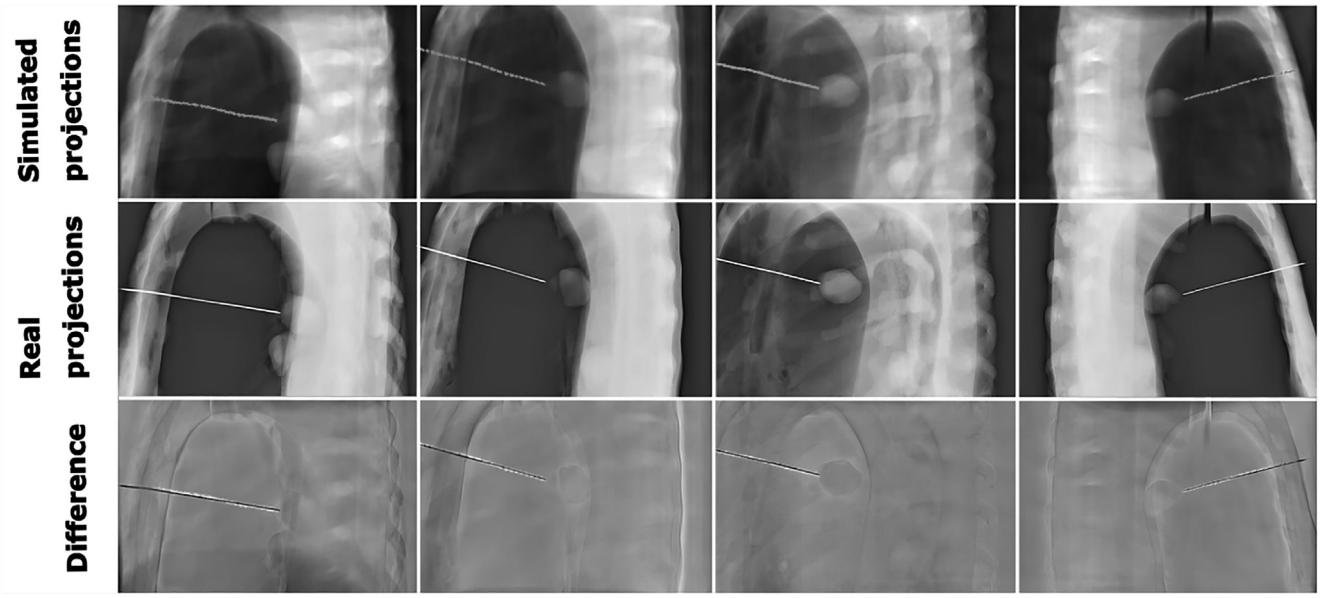

Figure 7. Some examples of simulated projections compared to real projections as well as a plot of the data residual (simulated versus measured projections) related to the optimized trajectory for target 2 using PICCS reconstruction and optimization method 1.

Fig. 7 shows some examples of simulated projections compared to real projections and a plot of residual data (simulation versus measured projections) related to the optimized trajectory for target 2 using PICCS reconstruction and optimization Method 1. Furthermore, Fig. 8 shows the simulated image compared to the real image for the same case (target 2 using PICCS reconstruction and optimization Method 1). A good agreement can be seen between the simulated projections and the real projections, and between the simulated image and the real reconstructed image.

Please cite this article as: S. Hatamikia, A. Biguri, G. Kronreif et al., Source-detector trajectory optimization for CBCT metal artifact reduction based on PICCS reconstruction, Z Med Phys, https://doi.org/10.1016/j.zemedi.2023.02.001

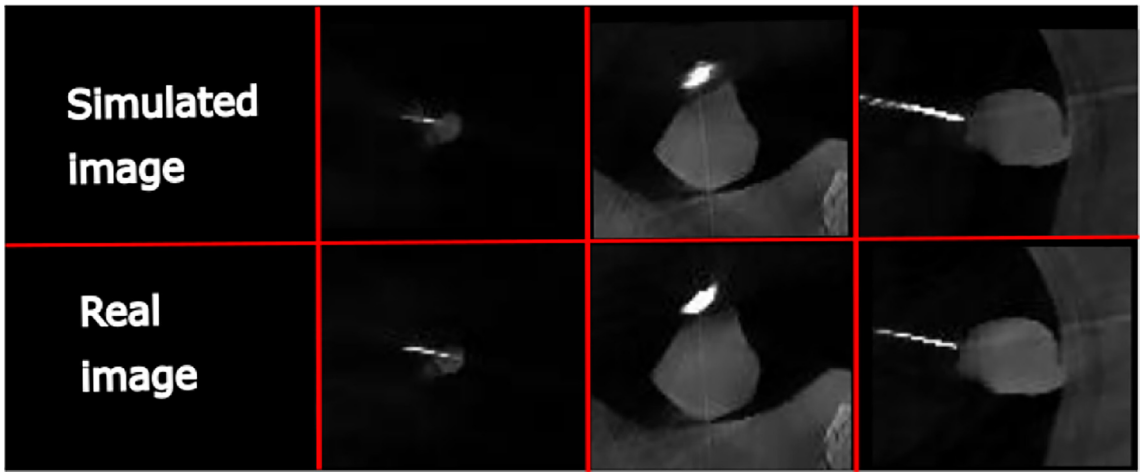

Figure 8. An example of a simulated image compared to the corresponding real image for optimized trajectory related to target 2 using PICCS reconstruction and optimization method 1.

4 Discussion

In this study, we proposed a framework for customized trajectory design in CBCT imaging with the goal of metal artifact reduction. The performance of sparse-view PICCS algorithm with optimized 3D trajectories was investigated for metal artifact reduction in needle-based interventions. We proposed to optimize out-of-plane rotations in 3D space and minimize projection views while reducing the metal artifacts at particular VOIs. In addition, the performance of the proposed method was evaluated for CBCT imaging under kinematic constraints when standard circular trajectories are not feasible. Our results based on two imaging targets inside an anthropomorphic thorax phantom with a biopsy needle inserted into a target, demonstrated that sparse-view optimized trajectories (20 projections) using PICCS algorithm achieved a significant higher image quality with respect to the reference C-arm circular trajectory using FDK method when using both 20 and even 313 projections. In addition, the results showed that the sparse-view optimized trajectories (20 projections, using PICCS algorithm) achieved a higher performance for most of the trajectory optimization methods as compared to the sparse-view circular trajectory reconstructed with PICCS (20 projections). This comparison confirms that trajectories including optimal 3D projection views can outperform the trajectories with standard-circular projections, highlighting the superiority of optimal 3D views over standard circular projection views in reducing metal artifacts.

Based on our knowledge, this is the first study which demonstrates the performance of metal artifact reduction using trajectory optimization for needle-based procedures. In addition, the use of PICCS to reduce metal artifacts in CBCT images is being investigated for the first time. The lower number of projections used makes our optimized trajectories suitable for low-dose CBCT interventions. Furthermore, considering that the proposed optimized trajectory is adaptable to spatially constrained situations and can enable CBCT under kinematic constraints, the achieved performance is very significant. We found that almost in all cases, all optimization methods improved the image performance compared to the standard circular trajectories. However, the trajectory optimization Method 3 showed the best performance among the 4 different optimization methods investigated in this study for both target 1 and target 2. The reason could be that this method is less constrained compared to other methods if good starting arcs are defined. Considering that this method provides a simple approach for trajectory optimization by combining the two best possible short arcs while achieving high performance in metal artifact reduction, it can be considered as a good candidate for future clinical implementation. In addition, using the same trajectory optimization method as in the previous study (Method 3) [19], we obtained a slightly higher UQI value (0.731 for target 1 and 0.725 for target 2) compared to the previous study, in which the authors reported a UQI of 0.703 for an anatomical phantom (without metal object) [19]. Furthermore, compared to the results of previous study [19], the proposed Methods 1 and 2 achieved comparable UQI values (0.693 and 0.708 for target 1, respectively), while we achieved a slightly higher UQI value (0.730) for target 1 using optimization Method 4 (greedy approach)

Please cite this article as: S. Hatamikia, A. Biguri, G. Kronreif et al., Source-detector trajectory optimization for CBCT metal artifact reduction based on PICCS reconstruction, Z Med Phys, https://doi.org/10.1016/j.zemedi.2023.02.001

from [22]. The UQI values were also comparable using Method 3 and Method 4 for target 1 (0.731 and 0.730, respectively). Direct comparison of the image quality metric from trajectory optimization Methods 1, 2 and 3 with the results reported in the study [22, Method 4] was not possible because of the different image quality metric used to report the results.

An important aspect of the clinical implementation of this approach is the consideration of possible movements of the target object that may occur during the scans in a clinical scenario. To incorporate this effect, we suggest considering a margin around the tumor (in the range of a few centimeters) as the VOI, assuring the region of interest to include the imaging target. In addition, a registration step will be required to have a practical workflow. This can be done using some initial projections and a two-dimensional 2D/3D registration to match the new position with the initial position (so that the needle has the same orientation as in the simulations) and adjust the trajectory accordingly on the fly. However, the effects of extended VOI and the inclusion of 2D/3D registration in the optimization process require further investigation and were not the focus of the current study. In this study, we realized the optimized trajectories using a step-and-shoot protocol by positioning the C-arm to each projection separately. This approach assumed a precise positioning of the source and detector. In a real clinical scenario, the motion of the C-arm gantry while positioning to new angles can lead to gantry wobble and therefore, a precise geometric calibration such as proposed in [32,33] should be considered for future implementation of this approach.

Our study mainly focuses on interventional procedures, especially percutaneous procedures such as needle biopsies, where a needle is usually the metal object. Applications such as pedicle screw insertion (e.g., in spine surgery), where multiple metal objects are commonly used, can also be considered as other important clinical scenarios that may benefit from the methods proposed in this study. Therefore, a future point of this research is to investigate the performance of the current methods for other types of procedures, such as screw placement with multiple metal objects. In this study, the execution time of different methods of trajectory optimization was between 3 and 11 minutes. We already have a fast optimization setup, but further improvements can be achieved by using multiple GPUs or other parallelization techniques. Therefore, it is realistic to expect that an adaptive and intraoperative trajectory optimization can be set up in a few minutes. This higher speed also opens the possibility to extend the search space to include a larger number of trajectories and other trajectory shapes, and to use advanced heuristic optimization techniques suitable for the trajectory optimization process.

5 Conclusion

We have shown that reduction of metal artifacts in needle-based procedures in CBCT imaging is possible using PICCS reconstruction and by optimizing out-of-plane rotations in 3D space while avoiding kinematic constraints. Our approach uses only 20 projections to reconstruct the image. This small number of projections not only significantly reduces metal artifacts, but can also contribute to a significant dose reduction in needle based CBCT interventions.

Declaration of Competing Interest

The authors declare that they have no known competing financial interests or personal relationships that could have appeared to influence the work reported in this paper.

Acknowledgement

This work has been supported by ACMIT—Austrian Center for Medical Innovation and Technology, which is funded within the scope of the COMET program and funded by Austrian BMVIT and BMWFW and the governments of Lower Austria and Tyrol. The authors have confirmed that any identifiable participants in this study have given their consent for publication. We are grateful for the local support in the angiographic suite in Wiener Neustadt provided by Gabi Flor and Corinna Dusek, MS. We also acknowledge the support of NVIDIA Corporation for the donation of Titan Xp GPU used for this research.

References

[1] Priya B et al. Application of Real-Time 3D Navigation System in CT-Guided Percutaneous Interventional Procedures: A Feasibility Study. Hindawi Radio Res Prac 2017:3151694.

[2] Yaniv Z, Cheng P, Wilson E, Popa T, Lindisch D, Campos-Nanez E, et al. Needle-based interventions with the image-guided surgery toolkit (IGSTK): from phantoms to clinical trials. IEEE Trans Biomed Eng 2010;57(4):922–933. https://doi.org/10.1109/TBME.2009.2035688, Epub 2009 Nov 17 PMID: 19923041.

[3] Daniel GS et al. Cone-Beam CT-Guided Lung Biopsies: Results in 94 Patient. Diagno 2020;10(12):1068.

[4] Kickuth R, Reichling C, Bley T, Hahn D, Ritter C. C-Arm Cone-Beam CT Combined with a New Electromagnetic Navigation System for Guidance of Percutaneous Needle Biopsies: Initial Clinical Experience. Rofo 2015;187(7):569–576. https://doi.org/10.1055/s-0034-1399313.

[5] Shi L, Robert Bennett N, Star-Lack J, Lu M, Wang AS. Projection-domain metal artifact correction using a dual layer detector, Proc SPIE Int Soc. Opt Eng 2020:11312. https://doi.org/10.1117/12.2547936.

Please cite this article as: S. Hatamikia, A. Biguri, G. Kronreif et al., Source-detector trajectory optimization for CBCT metal artifact reduction based on PICCS reconstruction, Z Med Phys, https://doi.org/10.1016/j.zemedi.2023.02.001

[6] Meilinger M et al. Metal artifact reduction in cone beam computed tomography using forward projected reconstruction information. Z Med Phys 2011;21(3):174–182.
[7] Zhang Y. Reducing metal artifacts in cone-beam CT images by preprocessing projection data. Int J Radiat Oncol Biol Phys 2007;67 (3):924–932.
[8] Gang GJ et al. Metal-Tolerant Noncircular Orbit Design and Implementation on Robotic C-Arm Systems. Conf Proc Int Conf Image Form Xray Comput Tomogr 2020:400–403.
[9] Gang GJ, Siewerdsen JH, Stayman JW. Non-circular CT orbit design for elimination of metal artifacts. Med imag 2020;11312:531–536.
[10] Hatamikia S et al. Source-detector trajectory optimization in cone-beam computed tomography: a comprehensive review on today's state-of-the-art. Phys Med Biol 2022;67:16TR03.
[11] Thies M et al. A learning-based method for online adjustment of C-arm Cone-beam CT source trajectories for artifact avoidance. Int J Comput Assist Radiol Surg 2020;15:1787–1796.
[12] Pengwei Wu et al. C-arm orbits for metal artifact avoidance (MAA) in cone-beam CT. Phys Med Biol 2020;65(16):165012. https://doi.org/10.1088/1361-6560/ab9454.
[13] Maier A et al. Discrete estimation of data completeness for 3D scan trajectories with detector offset. In Bildverarbeitung fur die Medizin 2015:47–52.
[14] Herl G, Hiller J, Thies M, Zaech JN, Unberath M, Maier A. Task-specific trajectory optimisation for twin-robotic x-ray tomography. IEEE Trans Comput Imag 2021;7:894–907.
[15] Bannas P, Li Y, Motosugi U, Li K, Lubner M, Chen GH, Pickhardt PJ. Prior Image Constrained Compressed Sensing Metal Artifact Reduction (PICCS-MAR): 2D and 3D Image Quality Improvement with Hip Prostheses at CT Colonography. Eur Radiol 2016;26 (7):2039–2046. https://doi.org/10.1007/s00330-015-4044-1.
[16] Humphriesa T, Wang J. Superiorized method for metal artifact reduction. Med Phys 2020;47(9):3984–3995.
[17] Lauzier P. Time-resolved cardiac interventional cone-beam CT reconstruction from fully truncated projections using the prior image constrained compressed sensing (PICCS) algorithm. Phys Med Biol 2012;57(9):2461–2476.
[18] Guang HC. Time-Resolved Interventional Cardiac C-arm Cone-Beam CT: An Application of the PI CCS Algorithm. IEEE Trans Med Imaging 2012;31(4):907–923.
[19] Hatamikia S et al. Optimization for customized trajectories in cone beam computed tomography. Med Phys 2020;47:4786–4799.
[20] Hatamikia S et al. Toward on-the-fly trajectory optimization for C-arm CBCT under strong kinematic constraints. PLOS ONE 2021. https://doi.org/10.1371/journal.pone.0245508.
[21] Sidky EY, Pan X. Image reconstruction in circular cone-beam computed tomography by constrained, total-variation minimization. Phys Med Biol 2008;53:4777–4807.
[22] Webster S et al. Task-based optimization of source-detector orbits in interventional cone-beam CT. Proc Int Meet Fully Three Dimensional Image Reconstruct Radiol Nucl Med 2015.
[23] Webster S et al. Task driven source-detector trajectories in cone-beam computed tomography: I. theory and methods. J Med Imag 2019;6(2):025002.
[24] Brierley N, Bellon C, Lazaro Toralles B. Optimized multi-shot imaging inspection design. Proc R Soc A 2018;474, 20170319 GA.
[25] Wang Z, Bovik SHR, Simoncelli EP. Image quality assessment: from error visibility to structural similarity. IEEE Trans Image Process 2004;13(4):600–612.
[26] Chou CY, Chuo YY, Hung Y, Wang W. A fast forward projection using multithreads for multirays on GPUs in medical image reconstruction. Med Phys 2011;38:4052–4065.
[27] Barrett JF, Keat N. Artifacts in CT: recognition and avoidance. Radio Graphics 2004;24:1679–1691.
[28] Meyer E, Raupach R, Lell M, Schmidt B, Kachelries M. Normalized metal artifact reduction (NMAR) in computed tomography. Med Phys 2010;37:5482–5493.
[29] Biguri A, Dosanjh M, Hancock S, Soleimani M. TIGRE: a MATLABGPU toolbox for CBCT image reconstruction. Biomed Phys Eng Express 2016;2:055010.
[30] Hatamikia S et al. Additively Manufactured Patient-Specific Anthropomorphic Thorax Phantom With Realistic Radiation Attenuation Properties. Front Bioeng Biotechnol 2020;8:385. https://doi.org/10.3389/fbioe.2020.00385.
[31] Zhang Z, Han X, Bian J, Manak J, Sidky EY, Pan X. Initial Experience in Image Reconstruction from Limited-angle C-arm CBCT Data. IEEE Nucl Sci Symp Conf Record 2011:3977–3979.
[32] Ouadah S et al. Self calibration of cone-beam CT geometry using 3D–2D image registration. Phys Med Biol 2016;61(7):2613–2632.
[33] Jacobson M. A line fiducial method for geometric calibration of cone-beam CT systems with diverse scan trajectories. Phys Med Biol 2018;2:025030.

Please cite this article as: S. Hatamikia, A. Biguri, G. Kronreif et al., Source-detector trajectory optimization for CBCT metal artifact reduction based on PICCS reconstruction, Z Med Phys, https://doi.org/10.1016/j.zemedi.2023.02.001